

A distal super enhancer mediates estrogen-dependent mouse uterine-specific gene transcription of *Igf1* (insulin-like growth factor 1)

Received for publication, April 5, 2019, and in revised form, May 6, 2019. Published, Papers in Press, May 9, 2019, DOI 10.1074/jbc.RA119.008759

Sylvia C. Hewitt^{†1}, Sydney L. Lierz[‡], Marleny Garcia[‡], Katherine J. Hamilton[‡], Artiom Gruzdev[§], Sara A. Grimm[¶], John P. Lydon^{||}, Francesco J. Demayo^{}, and Kenneth S. Korach[‡]**

From the [‡]Receptor Biology Group, [§]Knockout Mouse Core Laboratory, and ^{**}Pregnancy & Female Reproduction Group, Reproductive and Developmental Biology Laboratory and the [¶]Integrative Bioinformatics Support Group, NIEHS, National Institutes of Health, Research Triangle Park, North Carolina 27709 and the ^{||}Department of Molecular and Cellular Biology, Baylor College of Medicine, Houston, Texas 77030

Edited by Joel M. Gottesfeld

Insulin-like growth factor 1 (IGF1) is primarily synthesized in and secreted from the liver; however, estrogen (E2), through E2 receptor α (ER α), increases uterine *Igf1* mRNA levels. Previous ChIP-seq analyses of the murine uterus have revealed a potential enhancer region distal from the *Igf1* transcription start site (TSS) with multiple E2-dependent ER α -binding regions. Here, we show E2-dependent super enhancer-associated characteristics and suggest contact between the distal enhancer and the *Igf1* TSS. We hypothesized that this distal super-enhancer region controls E2-responsive induction of uterine *Igf1* transcripts. We deleted 430 bp, encompassing one of the ER α -binding sites, thereby disrupting interactions of the enhancer with gene-regulatory factors. As a result, E2-mediated induction of mouse uterine *Igf1* mRNA is completely eliminated, whereas hepatic *Igf1* expression remains unaffected. This highlights the central role of a distal enhancer in the assembly of the factors necessary for E2-dependent interaction with the *Igf1* TSS and induction of uterus-specific *Igf1* transcription. Of note, loss of the enhancer did not affect fertility or uterine growth responses. Deletion of uterine *Igf1* in a PgrCre;*Igf1*^{f/f} model decreased female fertility but did not impact the E2-induced uterine growth response. Moreover, E2-dependent activation of uterine IGF1 signaling was not impaired by disrupting the distal enhancer or by deleting the coding transcript. This indicated a role for systemic IGF1, suggested that other growth mediators drive uterine response to E2, and suggested that uterine-derived IGF1 is essential for reproductive success. Our findings elucidate the role of a super enhancer in *Igf1* regulation and uterine growth.

Insulin-like growth factor 1 (IGF1)² is primarily secreted from the liver (1) and circulates in serum bound to IGF1-binding proteins, which serve to regulate availability of IGF1 to its transmembrane receptor, IGF1R (2). IGF1 binding to the extracellular IGF receptor activates intracellular mitogen-activated protein kinase and phosphatidylinositol 3-kinase signaling pathways (3). Rodent uterine *Igf1* transcript is increased by E2, with a peak of induction 4–6 h following acute E2 injection, unlike the earliest responding uterine transcripts, such as *Fos*, which exhibit peak induction 1–2 h after E2 injection (4–7). E2 initiates a growth response in the epithelial cells of the rodent uterus. Numerous studies support a mechanism in which growth factors, including IGF1, are induced by E2 through the estrogen receptor α (ER α) and secreted from uterine stromal cells, subsequently activating growth factor receptor signaling of adjacent epithelial cells in a paracrine manner, leading to their proliferation. A precise approach that supports this mechanism is the selective deletion of ER α from uterine epithelial cells using Wnt7aCre;Esrr1^{fl/fl} mice or from anti-mesometrial stromal cells using Amhr2Cre;Esrr1^{fl/fl} mice. Administering E2 to Wnt7aCre;Esrr1^{fl/fl} mice results in uterine epithelial cell proliferation (8), whereas E2 treatment of Amhr2Cre;Esrr1^{fl/fl} mice causes proliferation only in those uterine epithelial cells that are adjacent to mesometrial stromal cells that still express ER α but not in anti-mesometrial epithelial cells adjacent to stromal cells where ER α has been deleted (9). Evaluation of the mouse uterine ER α cisome using ChIP-seq revealed ER α binding proximal to the two transcription start sites (TSSs) at the two *Igf1* alternate first exons (exons 1 and 2); however, an upstream enhancer region 40–70 kb 5' of the *Igf1* TSS exhibited very strong ER α binding (5, 10). Based on ranked acetylation of histone H3 lysine 27 (H3K27Ac) ChIP-seq enrichment, this distal *Igf1* can be classified as a super enhancer (11). We hypothesize that this distal super-enhancer region controls the E2-respon-

This research was supported in part by the Intramural Research Program of the National Institutes of Health, National Institute of Environmental Health Sciences 1ZIAES070065 (to K. S. K.). The authors declare that they have no conflicts of interest with the contents of this article. The content is solely the responsibility of the authors and does not necessarily represent the official views of the National Institutes of Health.

This article contains Table S1 and Figs. S1 and S2.

The data discussed in this publication have been deposited in NCBI's Gene Expression Omnibus and are accessible through GEO Series accession number GSE125972.

[†] To whom correspondence should be addressed. Tel.: 984-287-4317; E-mail: Sylvia.hewitt@nih.gov.

This is an open access article under the CC BY license.

9746 J. Biol. Chem. (2019) 294(25) 9746–9759

² The abbreviations used are: IGF, insulin-like growth factor; IGF1R, IGF1 receptor; ER α , estrogen receptor α ; TSS, transcription start site; Pol, RNA polymerase; ANOVA, analysis of variance; eRNA, enhancer RNA; V, vehicle; ERE, estrogen-responsive element; qPCR, quantitative PCR; nt, nucleotide(s); seq, sequencing; LSD, least significant difference; FPKM, fragments per kilobase of transcript per million mapped reads; HiC, chromatin capture sequencing.

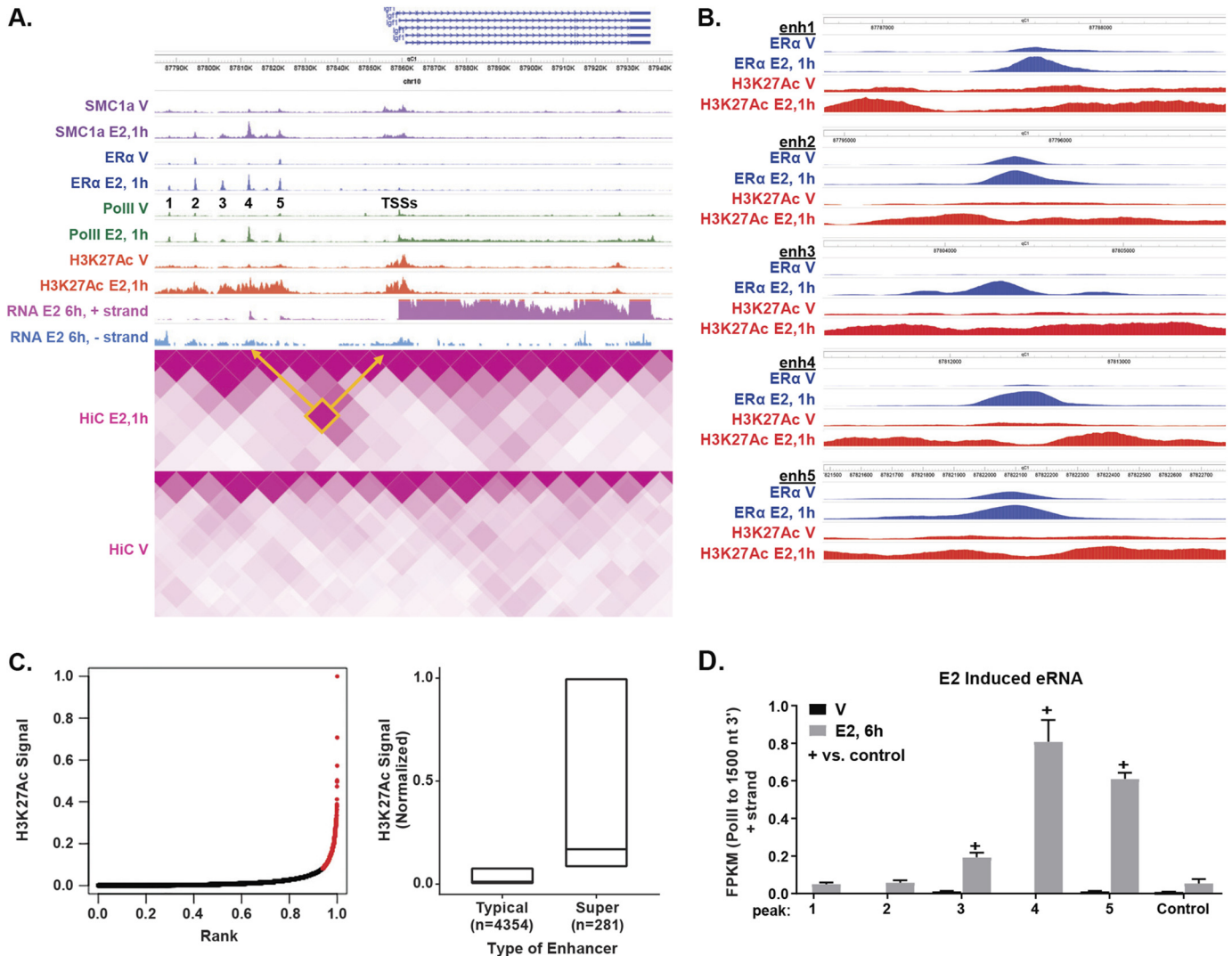


Figure 1. Enhancer-associated characteristics of a region 50–70 kb 5' of *Igf1* TSSs. A, screen shot (Wash U Epi Genome Browser) of the potential distal enhancer region. Tracks include SMC1a ChIP-seq of mouse uterus from V- or E2-treated samples and five E2-induced peaks of RNA PolII ChIP-seq that co-localize with E2-induced H3K27Ac and ERα ChIP-seq enrichment. The peaks are numbered 1–5. Stranded total RNA-seq from total mouse uterus RNA with E2-induced positive strand eRNA transcribed from peaks 3, 4, and 5 are noted. In the HiC heat map, the arrows indicate interactions between enhancer and TSS. See also Fig. S1 (A and B). B, focus on ERα ChIP-seq and H3K27Ac at each enhancer peak, 1–5. C, ranked H3K27Ac signal at 4600 ERα-binding regions. Red points beyond the elbow of the signal curve where slope = 1 are classified as super enhancers. The box plot shows normalized H3K27Ac signal at typical versus super enhancers, with mean indicated. D, signal strength (FPKM) of + strand RNA-seq from PolII local maximum to 1500 nt 3', at enhancer peaks 1–5. The data are represented as means ± S.E. (n = 3/peak) and at five control regions between peaks (n = 15) of V or E2 6-h samples. Data were analyzed using ANOVA with Fisher's False Discovery Rate (FDR) post test. +, p < 0.01 versus control region. See also Fig. S1B.

sive induction of uterine *Igf1* transcript via a looping mechanism by which the distal regions are brought into close contact with each other to facilitate induction of the *Igf1* transcript. We tested whether such deletion would subsequently result in loss of ERα-stimulated growth. Here, we report studies that evaluate the distal *Igf1* super enhancer and its roles in *Igf1* transcriptional regulation and uterine growth response.

Results

Super enhancer-associated characteristics of region distal from *Igf1* TSS

Our previous findings described a potential enhancer region 40–70 kb 5' of the *Igf1* TSS that exhibited E2-dependent ERα and RNA polymerase II (PolII) binding to five discrete regions (10); we designated these ERα-binding peaks IGF1 enhancers

1–5 (Fig. 1A and Fig. S1A). To further assess potential enhancer activity of this region, we evaluated several histone H3 modifications, including monomethylation of histone H3 lysine 4 (H3K4Me₁) and trimethylation of histone H3 lysine 4 (H3K4Me₃). Increased ratios of H3K4Me₁ to H3K4Me₃ are often associated with enhancers, whereas decreased ratios are often observed at promoters (12–14). We also examined acetylation of histone H3 lysine 27 (H3K27Ac) found in both enhancer and promoter regions (12, 15). The two enhancer-associated modifications (high H3K4Me₁/H3K4Me₃ ratio and presence of H3K27Ac) were apparent in the *Igf1* enhancer region (Fig. 1, A and B, and Fig. S1A). Furthermore, E2 treatment increased enhancer-associated H3K27Ac. We ranked the H3K27Ac ChIP-seq signal at 4600 ERα-bound regions to define ERα-binding super enhancers and classified this region as a

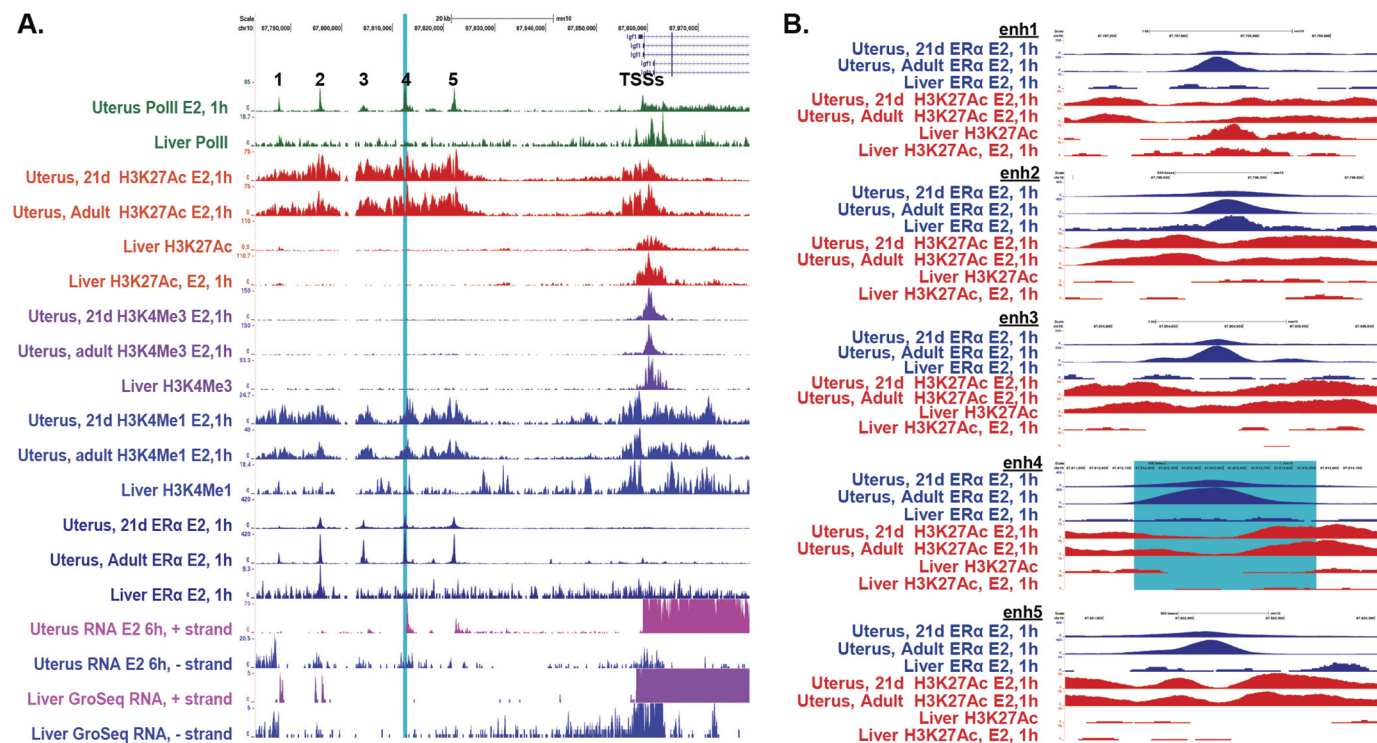


Figure 2. *Igf1* distal region develops as a super enhancer in uterine but not in liver tissue. A, UCSC Genome Browser screenshot of the *Igf1* distal enhancer region and TSSs with comparison of liver and uterus ChIP-seq data. Shown are PolII ChIP-seq (green) from ovariectomized female uterus injected with E2 (GEO GSE36455 (10)) and from adult male liver (GEO GSE49847 (18)); H3K27Ac ChIP-seq (red) from 21-day-old or ovariectomized adult female uterus (this study) or liver (GEO GSE70346 (17)) treated with E2 or female liver (GEO GSE44571 (16)); H3K4Me₃ ChIP-seq (purple) and H3K4Me₁ ChIP-seq (blue) from 21-day-old or ovariectomized adult female uterus treated with E2 (this study) or female liver (GEO GSE44571 (16)); ERα ChIP-seq (dark blue) from 21-day-old or ovariectomized adult female uterus (GEO GSE36455 (10)) or liver (GEO GSE70346 (17)) treated with E2; and stranded RNA-seq positive strand (pink) and negative strand (blue) from ovariectomized female uterus treated with E2 (this study) or GroSeq from adult male liver (GEO GSE59486 (19)) sample ZT16 collected 4 h after lights off. Enhancer 4 is highlighted in blue. B, focus on ERα and H3K27Ac ChIP-seq at each enhancer peak, 1–5.

super enhancer, ranked 97th of 281 super enhancers (Fig. 1C). Promoter-associated modifications (H3K27Ac and H3K4Me₃) are detected near the *Igf1* TSSs (Fig. 1A and Fig. S1A). Transcription of enhancer RNA (eRNA) is characteristic of transcriptional enhancers. Therefore, we used stranded RNA-seq of total uterine RNA to calculate signal strength fragments per kilobase of transcript per million mapped reads (FPKM) within 1500 bp 5' (– strand) or 3' (+ strand) of PolII of each of the two *Igf1* TSSs, the five enhancers, and a control region that lacked PolII (Fig. 1D and Fig. S1, A and B). E2 treatment of the mice results in robustly increased signal from the positive strand of the TSS. E2 also significantly increased signal from enhancers 3, 4, and 5 that returned to basal level by 24 h (Fig. 1D and Fig. S1, A and B).

To impact transcription of *Igf1*, the distal super enhancer must physically interact with the TSSs. We therefore analyzed samples from vehicle (V)- or E2-treated uterine tissue using chromatin capture sequencing (HiC), which indicated an interaction between the *Igf1* super-enhancer region and the *Igf1* TSS (Fig. 1A and Fig. S1A). We also examined binding of the cohesin subunit, SMC1a, using ChIP-seq and observed an E2-dependent increase of cohesin binding to enhancer 4 (Fig. 1A and Fig. S1A), consistent with the interaction detected using HiC. Observation of the super enhancer-associated modifications and contact suggests the distal region is bound by ERα and forms a loop enabling transcriptional regulation of *Igf1*.

Evaluation of PolII, H3K27Ac, H3K4me₃, and H3K4me₁ ChIP-seq from published liver data sets indicates this region lacks the super enhancer characteristics seen in the uterus (Fig. 2, A and B; GEO GSE44571 (16), GSE70346 (17), and GSE49847 (18)). In mouse liver samples, H3K27Ac is associated with peak 1, and moderate H3K4Me₁/H3K4Me₃ is seen (Fig. 2, A and B). GroSeq data from mouse liver reveals eRNA synthesis from an enhancer 1 and 2–positive strand and enhancer 1–negative strand (Fig. 2A; GEO GSE59486 (19)), indicating that this region of the enhancer may have some activity in the liver. ERα ChIP-seq from mouse liver revealed a small amount of ERα binding to enhancer 2 (Fig. 2, A and B; GEO GSE70346), indicating that enhancer 2 was less likely to modulate uterine-specific regulation. We also note that the ERα binding and histone modifications seen in adult ovariectomized uterine samples is apparent in prepubertal (21-day-old) uterine samples (Fig. 2, A and B), indicating that this region is developmentally programmed to function as an ERα-binding super enhancer in uterine cells, but not in liver tissue.

Constitutive ERα binding prior to E2 treatment was seen in the uterus at enhancers 2 and 5 (Fig. 1, A and B), indicating that these two enhancers were less likely to mediate E2 induction. We selected enhancer 4 for deletion via CRISPR Cas9-mediated genetic disruption, because it exhibited ERα and PolII binding, eRNA synthesis as well as the enhancer-associated histone modification H3K27Ac, and interaction with the TSS, and all these characteristics were E2-dependent.

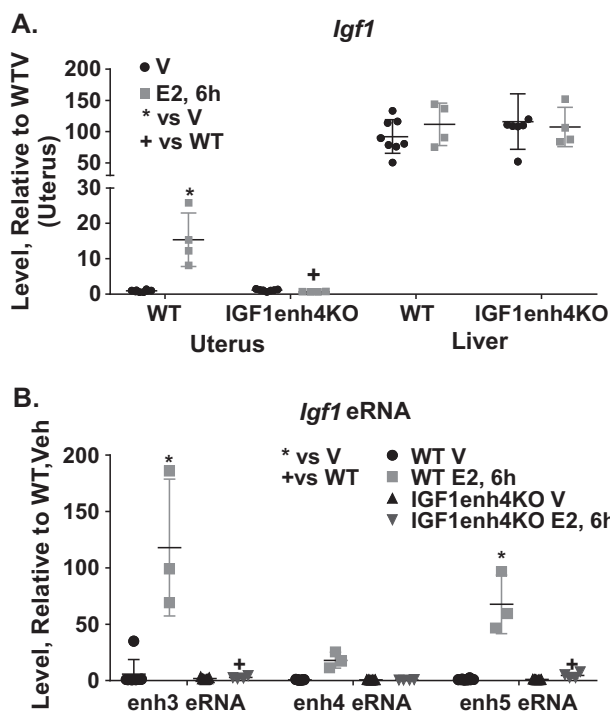


Figure 4. Deletion of *Igf1* enhancer 4 eliminated E2 induction of uterine *Igf1* mRNA and IGF1enh3, 4, and 5 eRNAs while preserving *Igf1* mRNA expression in the liver. A, expression levels of *Igf1* mRNA were analyzed by RT-PCR of total RNA isolated from uterus or liver tissue samples. Tissue samples were collected 6 h after injection of either saline (V) or E2. Samples were taken from mice with deletion of IGF1enh4 (IGF1enh4KO) or their WT littermates. The experiment was done twice. The data were plotted relative to WT V uterus = 1. The data are represented as means \pm S.D. V versus E2 values were tested using two-way ANOVA with Fisher's LSD post test. *, $p < 0.0001$, WT V $n = 8$, WT E2 $n = 4$, IGF1enh4KO V $n = 7$, and IGF1enh4KO E2 $n = 4$ samples (individual uterus)/group. B, IGF1enh3, 4, and 5 eRNAs analyzed by RT-PCR of total RNA isolated from uterus from ovariectomized female mice. Tissue samples were collected 6 h after injection of either saline (V) or E2. Samples were taken from mice with deletion of IGF1enh4 (IGF1enh4KO) or their WT littermates. The experiment was done twice. The data were plotted relative to WT V uterus = 1. The data are represented as means \pm S.D. V versus E2 values were tested using two-way ANOVA with Fisher's LSD post test. *, $p < 0.0001$, WT V $n = 8$, WT E2 $n = 4$, IGF1enh4KO V $n = 7$, and IGF1enh4KO E2 $n = 4$ samples (individual uterus)/group.

Deletion of IGF1 enhancer 4 selectively disrupts uterine *Igf1* induction

To test the effect of the ER α -binding site, we deleted 430 bp of DNA comprising the ER α -binding peak of IGF1 enhancer 4 (Fig. 3), generating IGF1enh4KO mice. To assess any impact deletion of the IGF1 enhancer 4 has on *Igf1* transcription, RNA was prepared from uteri and livers of ovariectomized mice that were treated with saline V or with E2 for 6 h for RT-PCR analysis. In WT mice, uterine *Igf1* RNA increased after E2 treatment (Fig. 4A), whereas the response was lost from IGF1enh4 KO uteri. *Igf1* is detected in WT and IGF1enh4KO liver RNA at comparable levels and is not significantly changed after E2 treatment of the mice (Fig. 4A). These findings indicate that deletion of *Igf1* enhancer 4 inhibits E2 induction of uterine *Igf1* mRNA without impacting expression of the *Igf1* gene in the liver. To ensure the disruption of IGF1enh4 did not affect uterine E2 transcriptional responses in general, we confirmed that two well characterized E2-induced uterine transcripts (*Fst* (Follistatin) and *Lif* (leukemia-inhibiting factor)), which are both expressed from epithelial cells, as well as the stromal gene

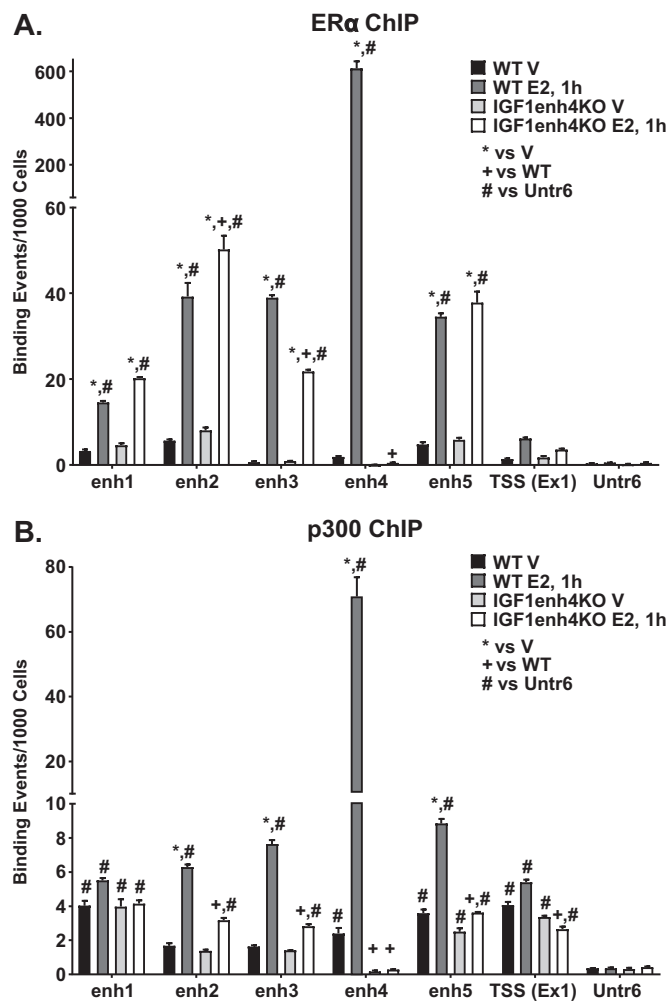


Figure 5. Deletion of *Igf1* enhancer 4 prevents ER α and p300 binding to the *Igf1* enhancer and TSS regions. ER α (A) and p300 (B) binding to the IGF1 enhancer region and to TSS was evaluated using ChIP-PCR of chromatin isolated from uterus samples of ovariectomized mice that were collected 1 h after injection of saline (V) or E2. Samples were taken from mice with deletion of IGF1enh4 (IGF1enh4KO) or their WT littermates. Baseline values are from Untr6, a Gene desert on chromosome 6. Enrichment is calculated as binding events/1000 cells, as described under "Experimental procedures." The data are represented as means \pm S.D. A pool of three uteri was used for each condition and tested in triplicate assays. V versus E2 values were tested using two-way ANOVA with Fisher's LSD post test. *, $p < 0.001$ versus V; +, $p < 0.0001$ versus WT; #, $p < 0.05$ versus Untr6.

Ramp3 (receptor activity-modifying protein 3), were induced 6 h after E2 treatment of IGF1enh4KO mice (Fig. S2).

We then used RT-PCR to confirm the presence and E2 induction of positive-strand eRNA transcripts from IGF1 enhancers 3, 4, and 5. All three eRNAs could be detected in uterine RNA (Fig. 4B) and were increased after E2 treatment. When IGF1enh4 was disrupted, the uterine eRNAs from enhancers 3, 4, and 5 were no longer increased by E2 treatment (Fig. 4B). The correlation of *Igf1* coding and eRNA induction in the uterus is consistent with a role for eRNA in facilitating transcription of *Igf1* mRNA.

IGF1 enhancer 4 orchestrates assembly of mediators of E2-dependent transcription

Next, we evaluated the impact of the enhancer deletion on the E2-dependent assembly of transcriptional mediators. Using

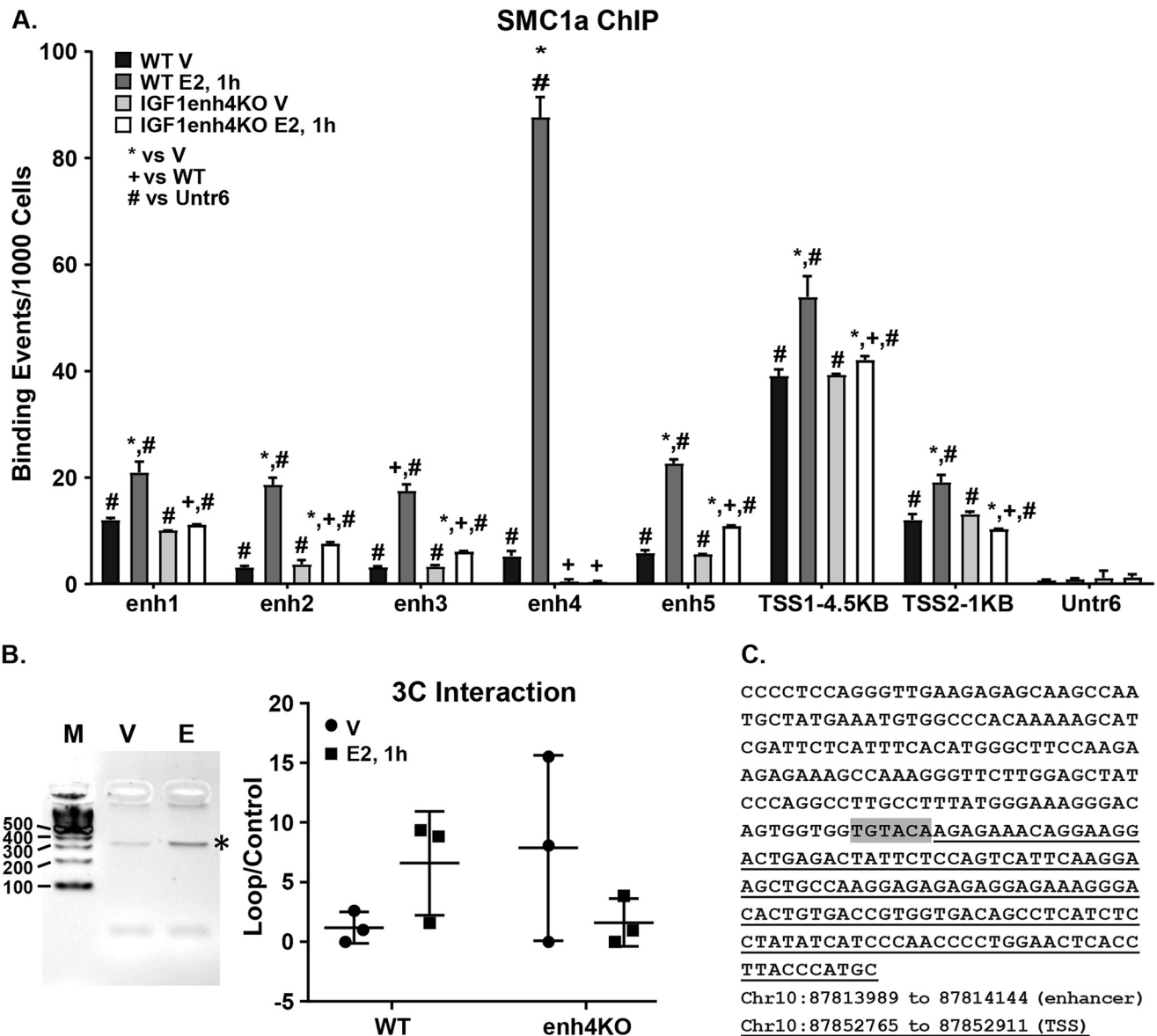


Figure 6. Deletion of *Igf1* enhancer 4 prevents SMC1a binding to *Igf1* enhancer and TSS regions. A, SMC1a (cohesin subunit) binding to the IGF1 enhancer region and to TSSs was evaluated using ChIP-PCR of chromatin isolated from uterus samples of ovariectomized mice that were collected 1 h after injection of saline (V) or E2. The samples were taken from mice with deletion of IGF1enh4 (IGF1enh4KO) or their WT littermates. Baseline values are from Untr6, a gene desert on chromosome 6. Enrichment is calculated as binding events/1000 cells, as described under "Experimental procedures." The data are represented as means \pm S.D. A pool of three uteri was used for each condition and tested in triplicate assays. V versus E2 (E) values were tested using two-way ANOVA with Fisher's LSD post test. *, $p < 0.001$ versus V; +, $p < 0.0001$ versus WT; #, $p < 0.05$ versus Untr6. B, interaction between IGF1enh4 and TSS was demonstrated using 3C-PCR. A 300-bp fragment (*) formed by ligation of BsrGI fragments was detected in WT samples and increased after E2 treatment. M indicates size markers, with sizes in bp. Graph of ratio of ligation band versus a control region band. C, sequencing the fragment confirmed that the band is a ligation product of fragments from the enhancer and TSS (underlined) regions ligated together at the BsrGI site (shaded gray). BLAST alignment of each part of fragment with mm10 coordinates is indicated.

ER α ChIP-PCR, we evaluated the impact of deletion of IGF1enh4 on ER α recruitment at IGF1enh1–5 and near the *Igf1* TSS in the uterus. Treatment of mice with E2 for 1 h increased ER α binding to chromatin at a site proximal to the *Igf1* TSS, as well as at IGF1enh1–5 (Fig. 5A). When IGF1enh4 is deleted, E2 still induces ER α binding to enhancers 1, 2, 3, and 5, yet *Igf1* transcription is not increased. This indicates that ER α binding to IGF1enh4 is critical for E2 induction of *Igf1* transcript in the uterus and that binding to the other sites is unable to compensate for the loss of the enhancer 4 site. Recruitment of p300 and its associated histone acetyltransferase activity to enhancers, and the TSS is indicative of enhanced transcription (20). There-

fore, we evaluated p300 association with IGF1enh1–5 and near the *Igf1* TSS in uterus samples. p300 binds the IGF1 TSS and IGF1enh1 (Fig. 5B), with a slight E2-dependent increase in WT mice. Treatment of WT mice with E2 for 1 h induced a pronounced increase in p300 associated with IGF1enh2–5. Administering E2 produced significantly less p300 binding at IGF1enh2–5 when IGF1enh4 was deleted and led to loss of the modest p300 increase at TSS and IGF1enh1. Therefore, IGF1enh4 appears to be critical for modulation of this key component of enhancer function and consequent eRNA synthesis needed to transduce the E2 response to the TSS. Interaction with cohesin is indicative of loop structure formation (21);

Table 1
6-Month continuous breeding trial

Cross: male × female	Litters/pair/6 months	Pups/pair/6 months	Pups/litter
WT × WT (<i>n</i> = 5)	4.2	22.8	5.45
WT × <i>Igf1</i> enh4KO (<i>n</i> = 5)	5.0	28.8	5.0
WT × <i>Igf1</i> tf (<i>n</i> = 5)	4.8	24.4	4.76
WT × PIGF cKO (<i>n</i> = 5)	2.4 ^a	8.6 ^a	3.33 ^a

^a *p* < 0.05 versus WT by one-way ANOVA.

therefore we compared cohesin subunit, SMC1a, interaction using ChIP-PCR. Prior to E2 treatment, SMC1a is prominently bound to a region ~4500 bp 5' of *Igf1* TSS1 (Fig. 6A). E2 treatment increases SMC1a interaction with all five IGF1 enhancers but most dramatically with IGF1 enhancer 4 (Fig. 6A). Deletion of this enhancer does not impact SMC1a binding to any sites prior to E2 treatment, except for the interaction with IGF1 enhancer 4 itself (Fig. 6A). Deletion of IGF1 enhancer 4 attenuates the E2-induced increase in SMC1a binding to all the enhancers and the TSSs (Fig. 6A), consistent with an impact on E2-dependent interaction between the super-enhancer region and the TSS. E2-dependent interaction between enh4 and the TSS in WT mice was confirmed using 3C-PCR (Fig. 6B). After E2 treatment, increased interaction could be detected. Interaction could also be detected in some of the enh4 KO samples (Fig. 6B), irrespective of E2 treatment. Thus, the interaction between the regions is not dependent on the enhancer 4 site. Sequencing of the PCR amplicon revealed a ligation of IGF1enh4 and TSS fragments (Fig. 6C).

Disrupting E2 induction of uterine *Igf1* does not impact fertility or uterine epithelial growth

Fertility of IGF1enh4KO females was assessed during a 6-month-long continuous breeding trial. IGF1enh4KO females were fertile, in terms of both the number of litters produced and the number of pups per litter (Table 1). We had expected that disrupting E2 regulation of uterine IGF1 would impact uterine function and fertility. To directly examine the impact of loss of uterine IGF1, we deleted the coding transcript. We used the PgrCre, which has Cre recombinase activity in all cells that express progesterone receptor, including all uterine cells (22). We bred PgrCre mice to mice with loxP sites flanking exon 4 of *Igf1* (23), which encodes the IGF1 peptide, to produce mice that lack IGF1 in uterine cells; we refer to these mice as “PIGFcKO.” Deletion of the *Igf1* coding transcript decreased female fertility after 6 months of continuous breeding (Table 1), with fewer litters and fewer pups per litter, indicating a requirement for uterine IGF1 for optimal fertility.

To further examine response within the uterine tissue, uterine epithelial cell growth was evaluated using the proliferation-associated marker, Ki67, 24 h after E2 treatment of ovariectomized mice. IGF1enh4KO and PIGFcKO females exhibited robust growth response that was similar to WT littermates (Fig. 7A). Previous work indicated a role for IGF1 in facilitating cell cycle progression, as uterine epithelial cells of IGF1 knockout mice that were treated with E2 exhibited G₂/M arrest (24). We assessed the ability of IGF1enh4KO and PIGFcKO uterine epithelial cells to undergo mitosis in response to E2 by using colchicine to trap and quantify mitotic cells. E2 increased mitotic

epithelial cells, shown by the mitotic marker phosphoserine 10 of histone H3 (Fig. 7, A and B).

RT-PCR revealed that E2 did not increase *Igf1* in PIGFcKO uterine sample (Fig. 7C), indicating successful deletion of the coding transcript. Uterine response to E2 after three daily injections results in dramatic increases in tissue weight and epithelial cell layer height. The response observed in IGF1enh4KO and PIGFcKO mice was a blunted response relative to WT, with significantly lower uterine weight (Fig. 7D). The height of the epithelial cell layer increased comparably with WT littermates (Fig. 7D). Overall, we observed similar responses when E2 induction of uterine *Igf1* was disrupted either by deleting the enhancer or the coding transcript.

Uterine *Igf1* disruption does not impair E2-induced uterine IGF1 receptor signaling

There is a long-standing debate regarding the relative contributions of systemic IGF1 (endocrine) and IGF1 synthesized within a tissue (paracrine/autocrine). Studies that support roles for systemic IGF1 in uterine response include the restoration of E2-mediated growth response following transplantation of IGF1 null uterine tissue into an IGF1 WT host (25). Such findings suggest that E2 increases VEGF in uterine tissue, leading to increased vascular permeability and influx of systemic IGF1 into the tissue (26, 27), and were further supported by a study using sFLT1-1, a VEGFa inhibitor, to prevent E2-induced uterine growth response (27). We next examined E2-initiated IGF1 receptor activation within uterine tissues of the two models with uterine IGF1 disruption. As has been previously noted by others (28), 6 h following E2 treatment, phosphorylated IGF1 receptor is detected in uterine tissue extracts (Fig. 8A). E2 increases uterine IGF1R phosphorylation in both the IGF1enh4KO and PIGFcKO (Fig. 8A) and also increases phosphorylation of AKT, which is a downstream target of IGF1R signaling (Fig. 8A). These findings support the concept that E2 facilitates the import of circulating IGF1 into the tissue. To directly assess whether E2 response included uptake of IGF1 into uterine tissue, an ELISA was used to measure IGF1 content in uterine homogenates. E2 increased the amount of IGF1 detected in uterine tissue (Fig. 8B), in WT mice but also in the PIGFcKO and IGF1enh4KO mice, which lack the E2 mediated increase of *Igf1* transcript. This finding is consistent with a role for E2 in facilitating entry of systemic IGF1 into uterine tissue.

Discussion

Our previous studies using deletion of uterine ERα from epithelial or anti-mesometrial stromal cells showed that epithelial cell ERα is dispensable but that stromal ERα is necessary for adjacent epithelial cell proliferative response induced by E2 (8, 9), supporting our hypothesis that ERα-mediated induction of growth factor synthesis in and secretion from stromal cells leads to growth of neighboring epithelial cells. IGF1 is an E2-induced stromal factor and thus is a candidate for a paracrine growth mediator. We were surprised, then, that E2 growth response is unimpaired when we prevent E2 induction of uterine IGF1; this indicates that paracrine factors other than IGF1 are involved in the response. FGF10 and BMP8a (29) have also

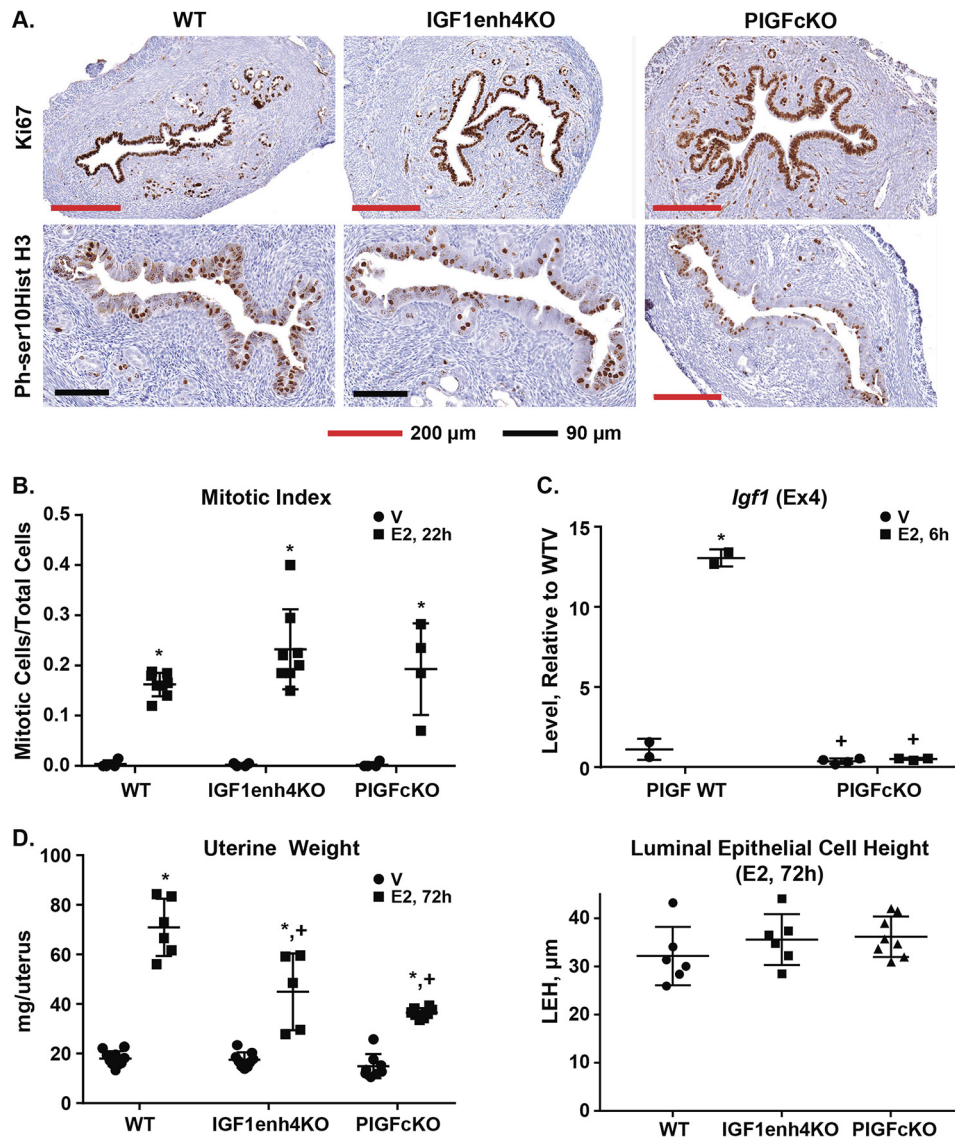


Figure 7. Disrupting uterine *Igf1* enhancer or coding transcript does not impair uterine growth. A, uterine cross-sections after immunohistochemical analysis of ovariectomized WT, IGF1enh4KO, or PIGFckO females that were treated with E2 for 24 h (Ki67) or treated with E2 for 22 h and colcemid for 2 h (phosphoserine 10 of histone H3; Ph-ser10Hist H3). B, mitotic index, calculated by counting proportion of epithelial cells that were positive for the mitotic marker of phosphoserine 10 of histone H3. C, expression levels of *Igf1* mRNA using primers targeting exon 4 analyzed by RT-PCR of total RNA isolated from uterus samples from ovariectomized female mice. Tissue samples were collected 6 h after injection of either saline (V) or E2. Samples were taken from mice with deletion of the *Igf1* coding transcript (PIGFckO) or their f/f littermates (PIGFWT). The data were plotted relative to WT V uterus = 1. The data are represented as means \pm S.D. *, $p < 0.001$ versus V; +, $p < 0.05$ versus WT. D, uterine weights of ovariectomized WT, IGF1enh4KO, or PIGFckO females that were treated with E2 daily for 3 days and then collected on the 4th day (E2, 72 h), $n = 5$ –10/group. *, $p < 0.0001$ versus V; +, $p < 0.0001$ versus WT. Height of luminal epithelial cell layer (LEH), measured in μ m.

been proposed to mediate uterine growth response and are expressed at comparable levels in WT and IGF1enh4KO uterine samples (data not shown) and may therefore be mediating uterine growth responses. Uterine-derived IGF1 does play a role in optimal response when E2 is administered for 3 days, because both IGF1enh4KO and PIGFckO showed an attenuated tissue weight increase with less fluid accumulation.

We were also somewhat surprised by the observation of normal fertility when we deleted the *Igf1* distal enhancer. Fertility of PIGFckO of females was significantly lower than Cre[−] littermates (Table 1), as evidenced by fewer and smaller litters. The PIGFckO ovary functions appeared to be normal, with normal estrous cycles and ovulation responses comparable with IGf/f (data not shown), suggesting impairment of their

uterine function led to the decreased fertility. In general, the fertility of PIGFckO females decreased over the course of the 6-month trial (data not shown), indicating that loss of uterine IGF1 may not prevent pregnancy *per se* but rather that uterine IGF1 may be needed for post-partum uterine recovery. The normal fertility of the IGF1enh4KO females indicates that E2-mediated uterine *Igf1* regulation is not necessary for fertility. *Igf1* expression is highest during diestrus (when progesterone is rising (30)) and proestrus (when estrogen and progesterone are elevated and ovulation is triggered by luteinizing hormone (30, 31)) and quite low during the estrous phase (when progesterone and estrogen are low and mating occurs (30, 31)) of the mouse estrous cycle (32). Together, these findings suggest other regulators of *Igf1*, including progesterone,

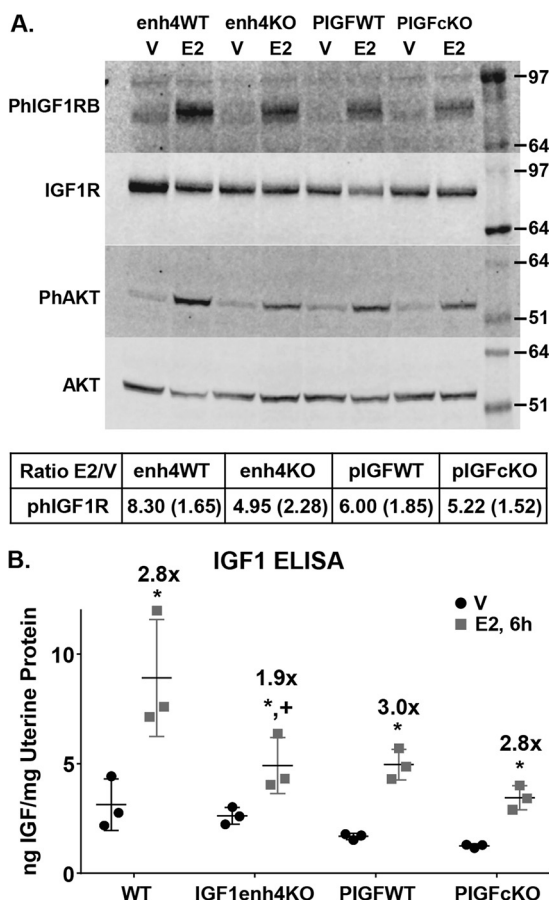


Figure 8. Uterine *Igf1* disruption does not impair E2-induced uterine IGF1 receptor signaling. *A*, representative Western blotting of uterine proteins demonstrates that E2 (6 h) induces activation of the IGF1R, as indicated by the phosphorylation of its B subunit (phIGF1RB; Tyr-1135/1136). The same blot was then reprobbed for total IGF1R. The same samples were analyzed for phosphorylation of AKT (phAKT; Ser-473) and AKT. Molecular masses of marker bands are shown in kilodaltons. PhIGF1RB was normalized to total IGF1R using a LI-COR Fc imager, and ratios of normalized phIGF1RB after E2 treatment relative to V treatment were calculated. Three pools of three uteri per sample were analyzed per group, and the average values \pm S.E. are shown in the table. *B*, ELISA for mouse IGF1 using uterine proteins. E2 induces increase in IGF1 protein within the uterine tissue, despite the disruption of induction of the *Igf1* transcript in the IGF1enh4KO and PgrCrexIgf1f/f models. Fold E2/V was calculated for each sample group and is shown above each E2 set ($n = 3$ pools of 3 uteri/sample). *, $p < 0.05$ versus V; +, $p < 0.001$ versus WT.

growth hormone, and STAT activators (33–35), may drive the expression of IGF1 needed for optimal uterine function.

Deleting E2-induced uterine IGF1, by disrupting the distal super enhancer (IGF1enh4KO), or by deleting the coding transcript (PIGFcKO) did not dramatically affect uterine response and function. Experimentally, our findings support the view that systemic endocrine IGF1, rather than IGF1 produced directly by uterine cells, is needed for E2 growth responses and fertility. However, findings that female mice with liver-specific disruption of IGF1 are fertile (36) but that global deletion of *Igf1* results in female reproductive problems (24) point to a more complex interplay of these systems. Observations indicating increased serum IGF1 levels are associated with better reproductive performance of cows (37) and that higher levels of serum IGF1 are associated with better IVF outcome (38) support a role for levels of systemic IGF1 in optimal reproductive function.

Interaction between distal enhancer regions and coding gene TSSs is proposed to be mediated by cohesin driven loop extrusion, which brings converging CCCTC-binding factor CTCF sites into contact (21). The resulting loop structure facilitates transcriptional regulation via mediator complexes, together with tissue specific transcription factors, including ER α (39). Estrogen-responsive element (ERE) motifs present in the IGF1enh4 sequence (Fig. 3B), as well as in the other binding peaks (10), serve to facilitate ER α binding. Other transcription factor-binding motifs are within the deleted DNA (Fig. 3C); some, such as HOX, FOX, and KLF, are known mediators of uterine transcriptional responses (40–42). We propose that ER α binding to enhancer 4 orchestrates assembly of transcriptional activators, as illustrated by the E2-dependent interaction with p300 (Fig. 5B). Although ER α binding to other sites was not impacted by deletion of enhancer 4 (Fig. 5A), p300 recruitment and consequent eRNA transcription from enhancers 3, 4, and 5 was disrupted. eRNA may serve to stabilize interaction between the distal super-enhancer region and the regulated gene's TSS via interaction between eRNA and mediator/cohesin subunits (43). Consistent with this view, we observe E2-dependent interaction of enhancer 4 with cohesin subunit SMC1a (Fig. 6A). The significance of eRNA transcription and its role in transcriptional regulation of coding transcripts is an emerging area of investigation. There is evidence that eRNA transcription may simply reflect the presence of PolII at enhancer regions (44). On the other hand, transcription of eRNA is involved in mechanisms of coding transcript regulation, because disrupting eRNA levels prevents regulation of its target transcripts (44, 45). Our findings are not sufficient to distinguish whether the eRNA *per se* or the process of its transcription is what is required for gene regulation. eRNA is widely reported to appear transiently, and consistent with this characteristic, the uterine eRNA transcripts detected return to basal levels within 24 h of E2 injection (Fig. S1, A and B). It is possible that deletion of any of the three eRNA-producing enhancers would impact *Igf1* transcription and that these three enhancers function as a unit. Our continuing studies will further elucidate mechanistic details that underlie the critical role of this distal super enhancer in uterine induction of *Igf1* transcription by E2. It is also interesting to note that this region develops as an ER α -binding super enhancer specifically in uterine tissue, as evidenced by enhancer-associated histone modifications and ER α binding in prepubertal uterine tissue and the lack of either in liver samples (Fig. 2).

Our observations have led us to conclude that uterine induction of *Igf1* mRNA after E2 treatment of mice is conferred by a distal super enhancer containing five ER α -binding sites. We have demonstrated the critical role of IGF1enh4 within this enhancer region in the E2 regulatory mechanism by showing that deletion of IGF1enh4 completely eliminates any increase in uterine *Igf1* transcript following E2 treatment. Overall our work indicates that a distal super enhancer is responsible for driving E2-dependent uterine induction of *Igf1* and that uterine-derived IGF1 is not required for pregnancy but is important for maintaining fertility.

Experimental procedures

Animals

All mice were used in accordance with an NIEHS-approved animal study protocol and using the 2015 edition of the Public Health Service Policy on Humane Care and Use of Laboratory Animals. IGF1enh4KO mice were made as described below. PgrCre;Igf1^{fl/fl} (PIGFcKO) mice were made by breeding PgrCre mice (22) (provided by Dr. Francesco J. DeMayo) with Igf1^{fl/fl} mice (23) (purchased from the Jackson Laboratory). For E2 response experiments, adult (10+ week old) female mice were ovariectomized and then housed for 10–14 days before the experiments to allow endogenous ovarian hormones to diminish. There was no blinding, and mice were randomly assigned to treatment groups. Homozygous PgrCre;Igf1^{fl/fl} or IGF1enh4KO were used in all studies, together with control (Igf1^{fl/fl} or WT, respectively) littermates. The mice were given a single intraperitoneal injection of 250 ng of E2 (Research Plus Inc., Barnegat, NJ) dissolved in 0.1 ml of normal saline. Control V animals were injected with 0.1 ml of normal saline. Tissue samples (uterus or liver) were collected 1, 2, 6, 22, or 24 h after the injections. For 3-day bioassays, the mice were subcutaneously injected daily with 250 ng of E2 dissolved in 0.1 ml of sesame oil (Sigma) for 3 days, and uterine tissue was collected on the 4th day. For the colchicine block experiment, demecolcine (Sigma; 100 μ g dissolved in 50 μ l of 10% ethanol, 90% water) was injected intraperitoneally 20 h after E2 or V injection, and tissue samples were collected 2 h later. Uterine tissue was weighed, a piece of the uterine horn was fixed in 10% formalin (Fisher Scientific), and the remainder was snap frozen in liquid nitrogen and then crushed into a powder using a metal pulverizer. Most uterine and liver samples were then used to isolate RNA as previously described (4). Some uterine samples were used to prepare protein extracts for Western blotting by homogenizing in 50 mM Tris, pH 7.5, 150 mM NaCl, 1% Triton X-100, 2.5 mg/ml sodium deoxycholate containing phosphatase inhibitor cocktails 2 and 3 (Sigma) and protease inhibitors (20 μ g/ml aprotinin (Sigma), 20 μ g/ml leupeptin (Sigma), and 4 μ g/ml α -phenylmethylsulfonyl fluoride (Calbiochem)). Other frozen uterine samples were shipped to Active Motif for H3K4Me1, H3K4Me3, or H3K27Ac HistonePath ChIP-seq or for SMC1a ChIP-seq or for ER α , p300, or SMC1a ChIP-PCR. For HiC, frozen uterine samples were shipped to Arima Genomics (San Diego, CA). For gene expression studies, at least three animals/group were used based on an at least 2-fold change, with CV = 0.2 and 90% power, tested by two-way ANOVA.

ChIP-seq

ER α V and E2 1 h and PolII ChIP-seq data sets were previously described and have been deposited in GEO (GSE36455) (10). E2 6-, 8-, and 12-h ER α ChIP-seq was done as described for previously published results (10). Histone and SMC1a ChIP-seq was done by Active Motif using the following Active Motif antibodies: 5 μ l of antibody 39297 for H3K4Me₁, 3 μ l of antibody 39159 for H3K4Me₃, or 8 μ l of antibody 39133 for H3K27Ac per 15 μ g of uterine chromatin and 4 μ g of antibody 61067 for SMC1a per 25 μ g of mouse uterine tissue chromatin.

Chromatin immunoprecipitation

Frozen mouse tissue was submersed in PBS + 1% formaldehyde, cut into small pieces, and incubated at room temperature for 15 min. Fixation was stopped by the addition of 0.125 M glycine (final). The tissue pieces were then treated with a TissueTearer and finally spun down and washed twice in PBS. Chromatin was isolated by the addition of lysis buffer, followed by disruption with a Dounce homogenizer. Lysates were sonicated, and the DNA was sheared to an average length of 300–500 bp. Genomic DNA (Input) was prepared by treating aliquots of chromatin with RNase, proteinase K, and heat for de-cross-linking, followed by ethanol precipitation. Pellets were resuspended, and the resulting DNA was quantified on a NanoDrop spectrophotometer. Extrapolation to the original chromatin volume allowed quantitation of the total chromatin yield.

An aliquot of chromatin (15 μ g for histone marks; 25 μ g for ER α) was precleared with protein A-agarose beads (Invitrogen). Genomic DNA regions of interest were isolated using 4 μ g of antibody. Complexes were washed, eluted from the beads with SDS buffer, and subjected to RNase and proteinase K treatment. Cross-links were reversed by incubation overnight at 65 °C, and ChIP DNA was purified by phenol-chloroform extraction and ethanol precipitation.

Quantitative PCRs (qPCRs) were carried out in triplicate on specific genomic regions using SYBR Green Supermix (Bio-Rad). The resulting signals were normalized for primer efficiency by carrying out qPCR for each primer pair using Input DNA.

Illumina sequencing libraries were prepared from the ChIP and Input DNAs by the standard consecutive enzymatic steps of end polishing, dA addition, and adaptor ligation. After a final PCR amplification step, the resulting DNA libraries were quantified and sequenced on Illumina's NextSeq 500 (75-nt reads, single end). All of the new data sets are deposited under GEO accession number GSE125972.

ChIP-PCR

The above steps for processing the tissue and performing the ChIP reactions were followed. Each ChIP reaction contained 30 μ g of tissue chromatin and 4 μ g of ER α antibody (Santa Cruz Biotechnologies, catalog no. sc-542) p300 antibody (Santa Cruz, catalog no. sc-585) or 10 μ l of SMC1a antibody (Active Motif, catalog no. 61067).

qPCRs were carried out in triplicate using SYBR Green Supermix (Bio-Rad, catalog no. 170-8882) on a CFX Connect™ real-time PCR system. One positive control site was tested (*Greb1* for ER α , *Sfswap* for p300, and *Lif* for SMC1a) and one negative control (Untr6), plus the test sites of interest. The resulting signals were normalized for primer efficiency by carrying out qPCR for each primer pair using input DNA (pooled unprecipitated genomic DNA from each sample). Active Motif's ChIP-qPCR normalization strategy, which considers the starting amount of chromatin, the final ChIP volume, and the primer efficiency, was used to calculate binding events per 1000 cells.

HiC

HiC experiments were performed by Arima Genomics (San Diego, CA) according to the Arima-HiC protocol described in the Arima-HiC kit. After the Arima-HiC protocol, Illumina-compatible sequencing libraries were prepared by first shearing purified Arima-HiC proximally ligated DNA and then size-selecting DNA fragments from ~200–600 bp using solid-phase reversible immobilization magnetic beads. The size-selected fragments were then enriched for biotin and converted into Illumina-compatible sequencing libraries using the KAPA Biosystems Hyper prep kit (Wilmington, MA). After adapter ligation, DNA was PCR-amplified and purified using solid-phase reversible immobilization beads. The purified DNA underwent standard quality checks (qPCR and Bioanalyzer) and was shipped to the NIEHS sequencing core. Libraries were loaded on an Illumina flow cell (Illumina, San Diego, CA) for paired-end 50-nucleotide read length sequencing on an Illumina NovaSeq instrument.

3C-PCR

3C-PCR was done using a modification of the method described in Ref. 46. One-fourth of a pulverized frozen uterus was cross-linked and homogenized, and nuclei were resuspended in 500 μ l of 1.2 \times New England Biolabs restriction buffer 2.1 (New England Biolabs) denatured with SDS and Triton X-100 and digested overnight with 400 units of BsrGI HF (New England Biolabs). Digestion was stopped with SDS, samples were diluted 10-fold with 1.1 \times New England Biolabs T4 ligation buffer, and Triton X-100 was added to neutralize the SDS. 1000 units of T4 ligase (New England Biolabs) was added, and samples were incubated for 4 h at 16 $^{\circ}$ C followed by 30 min at room temperature. DNA was isolated and analyzed by PCR using RedTaq mix (Sigma) and primers to detect the ligation product (see Table S1) and analyzed on a 3% GenePure agarose gel (GenePure, Kaysville, UT). The ligation product was purified using QiaQuick PCR kit (Qiagen) and sequenced by Genewiz (Morrisville, NC).

CRISPR CAS

Two CAS9 sgRNA (TAGCCCTTCATGCATCAGATNGG and AGAGGTCTACGTCACTACACNGG) were designed to excise the enhancer element. Complementary oligonucleotides were ordered from IDTDNA (Coralville, IA), cloned into a T7 sgRNA plasmid, and *in vitro* transcribed using Epicenter AmpliScribe T7 high-yield transcription kit (Madison, WI). C57BL/6J one-cell embryos were microinjected with both guides (10 ng/ μ l each) and 5' capped and poly(A) tailed Cas9 RNA (100 ng/ μ l) derived from pCAG-T3-hCAS-pA, a gift from Wataru Fujii and Kunihiko Naito (47). Microinjected embryos were surgically transferred to SWISS pseudo-pregnant females. At weaning, potential founders were genotyped by PCR and amplicon sequencing (IGF1_En4 forward, 5'-TGTTCAACAG-ACCTTCCGAGC-3'; reverse, 5'-CAGGCAGTGTAGTTTT-CAACCTG-3'). Founders of interest were bred to WT C57BL/6 mice, and F1 offspring were rescreened to confirm germ-line transmission. Phenotyping was done with founder line 3-7, which carries a 432-bp deletion between the two guides used, corresponding to chr10:87,812,231–87,812,662 (GRCm38/mm10

assembly). Correct deletion was confirmed by sequencing; the deleted sequence is shown in Fig. 3. In experiments, the mice with homozygous deletion (IGF1enh4KO) and their WT littermates were used. Mouse genotyping was subsequently done with either the screening primers above or primer/probe assay by Transnetix (WT forward, 5'-CACACACACAGACCCTAAATGGT-3'; WT reverse, 5'-CCCCTGACATCTCTGTGATCCT-3'; WT probe, 5'-CATGCCGCCCTGCCCT-3'; KO forward, 5'-GTTCTTCC-CTCACTGGTAAATGGA-3'; KO reverse, 5'-GCGCTCAGGG-ATAGCAAGAAG-3'; KO probe, 5'-CTGCAGTGGACTC-TCA-3').

RNA-seq

Uterine RNA from mice treated with V or with E2 for 2, 6, or 24 h was isolated using miRNeasy mini kit (Qiagen) according to the manufacturer's protocol and treated with DNase (Qiagen). RNA was sent to the National Institutes of Health Intramural Sequencing Center for stranded sequencing library preparation and sequencing. Stranded RNA-seq libraries were constructed from 1 μ g of total RNA after rRNA depletion using Ribo-Zero GOLD (Illumina, San Diego, CA). The Illumina TruSeq stranded total RNA sample prep kit was used according to the manufacturer's instructions except where noted. Amplification was performed using 10 cycles optimized for the input amount and to minimize the chance of overamplification. Unique barcode adapters were applied to each library. Libraries were pooled together for sequencing. The pooled libraries were sequenced on multiple lanes of a HiSeq2500 using version 4 chemistry to achieve a minimum of 55 million 125-base read pairs. The data were processed using RTA version 1.18.64 and CASAVA 1.8.2.

RNA-seq data processing

Libraries were sequenced as paired-end 126-mers on an Illumina HiSeq2500. Read pairs were filtered based on a mean base quality score >20. Filtered read pairs were mapped to the mm10 reference genome with STAR version 2.5 (48) (parameters –outMultimapperOrder Random –outSAMattrIHstart 0 –outFilterType BySJout –alignSJoverhangMin 8 –limitBAMsortRAM 55000000000 –outSAMstrandField intronMotif –outFilterIntronMotifs RemoveNoncanonical). Stranded depth tracks were generated by STAR version 2.5 (parameters –outWigType bedGraph –outWigStrand Stranded –outWigNorm None) and subsequently normalized by size factors reported from DESeq2 (49).

eRNA analysis

Under each ER α peak of interest, the local maxima of PolII ChIP-seq signal (WT, E2 treatment condition) was identified. Additionally, the midpoint between each pair of consecutive local maxima were selected as control sites. Evaluated regions were defined as 1500-nt windows 5' (– strand) or 3' (+ strand) of the selected PolII max (or control) sites, and the FPKM of each region was calculated per sample from strand-specific RNA-seq data.

ChIP-seq data processing

PolII ChIP-seq libraries were sequenced as single-end 36-mers by Active Motif. ER α ChIP-seq libraries were

sequenced as single-end 36- or 50-mers by Active Motif and then trimmed to a consistent length of 36 nt. Histone modification ChIP-seq libraries (H3K27ac, H3K4me1, and H3K4me3) were sequenced as single-end 75-mers on an Illumina NextSeq500. SMC1a ChIP-seq libraries were sequenced as single-end 75-mers by Active Motif on an Illumina NextSeq500. All reads were filtered to retain only those with mean base quality score >20. Adapter was removed from SMC1a samples by cutadapt version 1.2.1 (DOI:10.14806/ej.17.1.200, parameters –a AGATCGGAAGAG –O 5 q 0) and then filtered to remove any reads less than 30 nt after adapter trimming. Filtered reads were mapped to the mm10 reference genome with Bowtie version 0.12.8 (50), allowing uniquely mapped alignments only. Duplicates were removed with MarkDuplicates.jar from the Picard tool suite (<http://broadinstitute.github.io/picard>).³ For visualization purposes, mapped reads were extended to their estimated fragment length (150 nt for PolII and ER α ; 200 nt for SMC1a and H3K27ac, H3K4me1, and H3K4me3 histone modifications), converted to bedGraph format via BEDTools genomeCoverageBed (51), and then normalized to either 15 million (for ER α) or 20 million (all others) uniquely mapped nonduplicate reads per sample.

Identification of super enhancers

Super enhancers were identified based on the method described by Bojcsuk *et al.* (11). First, ER α peak calls with high stringency were called by HOMER (parameters –fdr 0.00001 –F 12 –style factor) for the ovariectomized adult and 21-day-old samples and then combined via BEDtools mergeBed (version 2.24.0). BEDtools mergeBed (version 2.24.0) was then rerun, this time to merge all peak calls within 12.5 kb. This set was subsequently filtered to retain only those regions with more than one contributing called peak. Each region was scored by counting the number of overlapping uniquely mapped nonduplicate reads with BEDtools multiBamCov (version 2.24.0); reads in this calculation were H3K27ac ChIP-seq data after extension of mapped read length to 200 nt. After normalizing to 20 million reads, the input-subtracted signal was determined per region. The signal curve was plotted as H3K27ac signal *versus* region rank and rescaled to span 0 to 1 on both axes. Definition of each region as a “typical enhancer” or “super enhancer” was determined according to the elbow of the signal curve where slope = 1.

HiC data processing

The Juicer (version 1.5.6) platform was used for processing the HiC samples (52). For each sample, a .hic file was generated based on mapped to the mm10 reference genome with restriction sites defined according to the Arima mixture of restriction enzymes. Chromatin loops were identified with the Juicer hiccup utility at default parameters.

RT-PCR

RNA was isolated from livers and uteri using TRIzol reagent, and then 1–2 μ g was treated with DNase (Invitrogen) and used

to synthesize cDNA using random hexamers (Applied Biosystems, Grand Island, NY) and Super Script II (Invitrogen) per the manufacturer's protocols. Resulting cDNA was diluted 1:10 (for eRNA real time PCR) or 1:100 (for mRNA real-time PCR) and analyzed using Fast SYBR Green Master Mix (Applied Biosystems). Primer sequences are listed in Table S1. The data were analyzed using the method described by Pfaffl (53).

Histology and immunohistochemical analysis

Formalin-fixed uterine tissue was embedded in paraffin, and 4- μ m sections were cut and mounted on charged slides. Luminal epithelial height was measured in hematoxylin- and eosin-stained sections on blinded images using ImageJ to draw and measure 5 lines/tissue section perpendicular to the luminal epithelial cell layer. For immunostaining, sections were deparaffinized and decloaked in antigen decloaker buffer (Biocare Medical, Pacheco, CA) in a pressurized decloaking chamber (Biocare Medical) for 3 min (Ki67) or 5 min (phosphohistone H3 (Ser-10)). Slides were incubated in 5% hydrogen peroxide (Fisher) for 15 min. For Ki67, slides were blocked with 10% horse serum (Jackson ImmunoResearch) in wash buffer (50 mM Tris (Lonza, Allendale, NJ), 4 mM NaCl (Lonza) with 0.5% Tween 20 (Amersham Biosciences) and then incubated with anti-Ki-67 (BD Pharmingen/BD Biosciences, San Jose, CA, catalog no. 550609) diluted 1:100 in 10% normal horse serum solution for 1 h, Biotinylated horse anti-mouse IgG (Vector Laboratories, Burlingame, CA) diluted 1:500 in wash buffer for 30 min, followed by extra avidin peroxidase (Sigma) diluted 1:50 in wash buffer for 30 min, with three 5-min washes with wash buffer between each step. Dako Liquid 3,3 diaminobenzidine (DAB) substrate (Agilent Technologies, Santa Clara, CA) was applied for 3 min, and the slides were counterstained with hematoxylin solution (Sigma), rinsed in wash buffer, dehydrated, and mounted with coverslips and Permount (Fisher). For phosphohistone H3 (Ser10), slides were blocked with 5% goat serum (Jackson ImmunoResearch) with 1% BSA (Sigma) in wash buffer for 20 min and then incubated with anti-phosphohistone H3 (Ser-10) (EMD Millipore catalog no. 06-570) diluted 1:500 in 5% goat serum with 1% BSA for 1 h, biotinylated goat anti-rabbit IgG (Vector Laboratories) diluted 1:500 in wash buffer for 30 min, followed by extra avidin peroxidase (Sigma) diluted 1:50 in wash buffer for 30 min. Dako liquid DAB substrate (Agilent Technologies) was applied for 6 min, and the slides were counterstained with hematoxylin solution (Sigma), rinsed in wash buffer, dehydrated, and mounted with coverslips and Permount (Fisher).

Western blotting

Uterine homogenates containing 40 μ g of protein were loaded on a 4–12% NuPAGE Bis-Tris gel (Thermo), separated with 1 \times MOPS running buffer (Thermo), and transferred to nitrocellulose membranes using an iBlot system (Thermo), all according to the manufacturer's directions. Nitrocellulose membranes were blocked for 1 h in Odyssey blocking buffer TBS (LI-COR, Lincoln, NE) and then incubated overnight at 4C with anti-phospho-IGF1 receptor β antibody (Cell Signaling Technologies, Danvers, MA, catalog no. 3024) diluted 1:1000 in Odyssey blocking buffer. Bands were detected with IRDye 800

³ Please note that the JBC is not responsible for the long-term archiving and maintenance of this site or any other third party hosted site.

anti-rabbit IgG (LI-COR) diluted 1:20,000 in Odyssey buffer for 1 h at room temperature, and data were collected using the LI-COR Fc imager. The blot was then stripped with LI-COR 1× stripping buffer and reprobed with IGF-I receptor β (Cell Signaling Technologies catalog no. 3018) diluted 1:1000 in 5% Blotto (Santa Cruz Biotechnologies, Dallas, TX) and detected with IRDye 680 anti-rabbit IgG (LI-COR). Separate blots were run with the same samples and probed with antibodies for phospho-Akt (Ser-473) antibody diluted 1:1000 in Odyssey blocking buffer (Cell Signaling Technologies, catalog no. 9721), stripped, and then reprobed with Akt antibody diluted 1:1000 in 5% Blotto (Cell Signaling Technologies, catalog no. 9272).

IGF1 ELISA

Serum or uterine homogenate IGF1 levels were determined using the ALPCO IGF-1 mouse/rat ELISA (ALPCO, Salem NH; catalog no. 22-IG1MS-E01). Serum was diluted 100-fold, and uterine homogenates were diluted 1:10 and assayed according to the protocol provided with the ELISA kit. Uterine homogenate results were normalized to total protein levels.

Author contributions—S. C. H. and A. G. conceptualization; S. C. H. and S. A. G. data curation; S. C. H., M. G., and S. A. G. formal analysis; S. C. H. and S. L. L. validation; S. C. H., S. L. L., M. G., and K. J. H. investigation; S. C. H., S. L. L., M. G., A. G., and S. A. G. visualization; S. C. H., K. J. H., A. G., and S. A. G. methodology; S. C. H., A. G., and S. A. G. writing—original draft; S. C. H., S. L. L., M. G., and K. S. K. project administration; S. C. H., S. L. L., K. J. H., A. G., S. A. G., and K. S. K. writing—review and editing; J. P. L., F. J. D., and K. S. K. resources; K. S. K. supervision; K. S. K. funding acquisition.

Acknowledgments—We thank Dr. Francesco J. DeMayo for providing the PgrCre mice. We also are grateful to Drs. Wipawee Winuthayanon and Harriet Kinyamu for discussions and critical reading of the manuscript. We greatly appreciate David Monroy for animal care; NIEHS surgeons Page Myers, David Goulding, and Chris McGee for ovariectomies; and the NIEHS Sequencing Core members Greg Solomon, Jason Malphurs, and Paul Wade and the NCI Sequencing Core for sequencing. We thank Paul Cacioppo of the NIEHS Office of Communications for compiling the figures into proper formats.

References

- Holt, R. I. (2002) Fetal programming of the growth hormone–insulin-like growth factor axis. *Trends Endocrinol. Metab.* **13**, 392–397 [CrossRef Medline](#)
- Clemmons, D. R. (2016) Role of IGF binding proteins in regulating metabolism. *Trends Endocrinol. Metab.* **27**, 375–391 [CrossRef Medline](#)
- Siddle, K. (2011) Signalling by insulin and IGF receptors: supporting acts and new players. *J. Mol. Endocrinol.* **47**, R1–R10 [CrossRef Medline](#)
- Hewitt, S. C., Deroo, B. J., Hansen, K., Collins, J., Grissom, S., Afshari, C. A., and Korach, K. S. (2003) Estrogen receptor-dependent genomic responses in the uterus mirror the biphasic physiological response to estrogen. *Mol. Endocrinol.* **17**, 2070–2083 [CrossRef Medline](#)
- Hewitt, S. C., Li, Y., Li, L., and Korach, K. S. (2010) Estrogen-mediated regulation of Igf1 transcription and uterine growth involves direct binding of estrogen receptor α to estrogen-responsive Elements. *J. Biol. Chem.* **285**, 2676–2685 [CrossRef Medline](#)
- Murphy, L. J., Murphy, L. C., and Friesen, H. G. (1987) Estrogen induces insulin-like growth factor-I expression in the rat uterus. *Mol. Endocrinol.* **1**, 445–450 [CrossRef Medline](#)

- Zhu, L., and Pollard, J. W. (2007) Estradiol-17 β regulates mouse uterine epithelial cell proliferation through insulin-like growth factor 1 signaling. *Proc. Natl. Acad. Sci. U.S.A.* **104**, 15847–15851 [CrossRef Medline](#)
- Winuthayanon, W., Hewitt, S. C., Orvis, G. D., Behringer, R. R., and Korach, K. S. (2010) Uterine epithelial estrogen receptor α is dispensable for proliferation but essential for complete biological and biochemical responses. *Proc. Natl. Acad. Sci. U.S.A.* **107**, 19272–19277 [CrossRef Medline](#)
- Winuthayanon, W., Lierz, S. L., Delarosa, K. C., Sampels, S. R., Donoghue, L. J., Hewitt, S. C., and Korach, K. S. (2017) Juxtacrine activity of estrogen receptor α in uterine stromal cells is necessary for estrogen-induced epithelial cell proliferation. *Sci. Rep.* **7**, 8377 [CrossRef Medline](#)
- Hewitt, S. C., Li, L., Grimm, S. A., Chen, Y., Liu, L., Li, Y., Bushel, P. R., Fargo, D., and Korach, K. S. (2012) Research resource: whole-genome estrogen receptor α binding in mouse uterine tissue revealed by ChIP-seq. *Mol. Endocrinol.* **26**, 887–898 [CrossRef Medline](#)
- Bojcsuk, D., Nagy, G., and Balint, B. L. (2017) Inducible super-enhancers are organized based on canonical signal-specific transcription factor binding elements. *Nucleic Acids Res.* **45**, 3693–3706 [Medline](#)
- Ko, J. Y., Oh, S., and Yoo, K. H. (2017) Functional enhancers as master regulators of tissue-specific gene regulation and cancer development. *Mol. Cells* **40**, 169–177 [Medline](#)
- Calo, E., and Wysocka, J. (2013) Modification of enhancer chromatin: what, how, and why? *Mol. Cell* **49**, 825–837 [CrossRef Medline](#)
- Kim, T.-K., and Whiekhart, R. (2015) Architectural and functional commonalities between enhancers and promoters. *Cell* **162**, 948–959 [CrossRef Medline](#)
- Lam, M. T., Li, W., Rosenfeld, M. G., and Glass, C. K. (2014) Enhancer RNAs and regulated transcriptional programs. *Trends Biochem. Sci.* **39**, 170–182 [CrossRef Medline](#)
- Sugathan, A., and Waxman, D. J. (2013) Genome-wide analysis of chromatin states reveals distinct mechanisms of sex-dependent gene regulation in male and female mouse liver. *Mol. Cell. Biol.* **33**, 3594–3610 [CrossRef Medline](#)
- Palierne, G., Fabre, A., Solinhac, R., Le Péron, C., Avner, S., Lenfant, F., Fontaine, C., Salbert, G., Flouriot, G., Arnal, J. F., and Métivier, R. (2016) Changes in gene expression and estrogen receptor cistrome in mouse liver upon acute E2 treatment. *Mol. Endocrinol.* **30**, 709–732 [CrossRef Medline](#)
- Yue, F., Cheng, Y., Breschi, A., Vierstra, J., Wu, W., Ryba, T., Sandstrom, R., Ma, Z., Davis, C., Pope, B. D., Shen, Y., Pervouchine, D. D., Djebali, S., Thurman, R. E., Kaul, R., et al. (2014) A comparative encyclopedia of DNA elements in the mouse genome. *Nature* **515**, 355–364 [CrossRef Medline](#)
- Fang, B., Everett, L. J., Jager, J., Briggs, E., Armour, S. M., Feng, D., Roy, A., Gerhart-Hines, Z., Sun, Z., and Lazar, M. A. (2014) Circadian enhancers coordinate multiple phases of rhythmic gene transcription *in vivo*. *Cell* **159**, 1140–1152 [CrossRef Medline](#)
- Holmqvist, P. H., and Mannervik, M. (2013) Genomic occupancy of the transcriptional co-activators p300 and CBP. *Transcription* **4**, 18–23 [CrossRef Medline](#)
- Rowley, M. J., and Corces, V. G. (2018) Organizational principles of 3D genome architecture. *Nat. Rev. Genet.* **19**, 789–800 [CrossRef Medline](#)
- Soyal, S. M., Mukherjee, A., Lee, K. Y., Li, J., Li, H., DeMayo, F. J., and Lydon, J. P. (2005) Cre-mediated recombination in cell lineages that express the progesterone receptor. *Genesis* **41**, 58–66 [CrossRef Medline](#)
- Liu, J. L., Grinberg, A., Westphal, H., Sauer, B., Accili, D., Karas, M., and LeRoith, D. (1998) Insulin-like growth factor-I affects perinatal lethality and postnatal development in a gene dosage-dependent manner: manipulation using the Cre/loxP system in transgenic mice. *Mol. Endocrinol.* **12**, 1452–1462 [CrossRef Medline](#)
- Adesanya, O. O., Zhou, J., Samathanam, C., Powell-Braxton, L., and Bondy, C. A. (1999) Insulin-like growth factor 1 is required for G₂ progression in the estradiol-induced mitotic cycle. *Proc. Natl. Acad. Sci. U.S.A.* **96**, 3287–3291 [CrossRef Medline](#)
- Sato, T., Wang, G., Hardy, M. P., Kurita, T., Cunha, G. R., and Cooke, P. S. (2002) Role of systemic and local IGF-I in the effects of estrogen on growth and epithelial proliferation of mouse uterus. *Endocrinology* **143**, 2673–2679 [CrossRef Medline](#)
- Kazi, A. A., Molitoris, K. H., and Koos, R. D. (2009) Estrogen rapidly activates the PI3K/AKT pathway and hypoxia-inducible factor 1 and in-

- duces vascular endothelial growth factor A expression in luminal epithelial cells of the rat uterus. *Biol. Reprod.* **81**, 378–387 [CrossRef Medline](#)
27. Hastings, J. M., Licence, D. R., Burton, G. J., Charnock-Jones, D. S., and Smith, S. K. (2003) Soluble vascular endothelial growth factor receptor 1 inhibits edema and epithelial proliferation induced by 17 β -estradiol in the mouse uterus. *Endocrinology* **144**, 326–334 [CrossRef Medline](#)
28. Richards, R. G., DiAugustine, R. P., Petrusz, P., Clark, G. C., and Sebastian, J. (1996) Estradiol stimulates tyrosine phosphorylation of the insulin-like growth factor-1 receptor and insulin receptor substrate-1 in the uterus. *Proc. Natl. Acad. Sci. U.S.A.* **93**, 12002–12007 [CrossRef Medline](#)
29. Chung, D., Gao, F., Jegga, A. G., and Das, S. K. (2015) Estrogen mediated epithelial proliferation in the uterus is directed by stromal Fgf10 and Bmp8a. *Mol. Cell. Endocrinol.* **400**, 48–60 [CrossRef Medline](#)
30. Walmer, D. K., Wrona, M. A., Hughes, C. L., and Nelson, K. G. (1992) Lactoferrin expression in the mouse reproductive tract during the natural estrous cycle: correlation with circulating estradiol and progesterone. *Endocrinology* **131**, 1458–1466 [CrossRef Medline](#)
31. Wang, H., and Dey, S. K. (2006) Roadmap to embryo implantation: clues from mouse models. *Nat. Rev. Genet.* **7**, 185–199 [CrossRef Medline](#)
32. Lee, D. S., Yanagimoto Ueta, Y., Xuan, X., Igarashi, I., Fujisaki, K., Sugimoto, C., Toyoda, Y., and Suzuki, H. (2005) Expression patterns of the implantation-associated genes in the uterus during the estrous cycle in mice. *J. Reprod. Dev.* **51**, 787–798 [CrossRef Medline](#)
33. Blumbach, K., Niehoff, A., Belgardt, B. F., Ehlen, H. W., Schmitz, M., Hallinger, R., Schulz, J. N., Brüning, J. C., Krieg, T., Schubert, M., Gullberg, D., and Eckes, B. (2012) Dwarfism in mice lacking collagen-binding integrins $\alpha 2\beta 1$ and $\alpha 11\beta 1$ is caused by severely diminished IGF-1 levels. *J. Biol. Chem.* **287**, 6431–6440 [CrossRef Medline](#)
34. Klover, P., and Hennighausen, L. (2007) Postnatal body growth is dependent on the transcription factors signal transducers and activators of transcription 5a/b in muscle: a role for autocrine/paracrine insulin-like growth factor I. *Endocrinology* **148**, 1489–1497 [CrossRef Medline](#)
35. Davey, H. W., Xie, T., McLachlan, M. J., Wilkins, R. J., Waxman, D. J., and Grattan, D. R. (2001) STAT5b is required for GH-induced liver IGF-I gene expression. *Endocrinology* **142**, 3836–3841 [CrossRef Medline](#)
36. Yakar, S., Liu, J. L., Stannard, B., Butler, A., Accili, D., Sauer, B., and LeRoith, D. (1999) Normal growth and development in the absence of hepatic insulin-like growth factor I. *Proc. Natl. Acad. Sci. U.S.A.* **96**, 7324–7329 [CrossRef Medline](#)
37. Falkenberg, U., Haertel, J., Rotter, K., Iwersen, M., Arndt, G., and Heuwer, W. (2008) Relationships between the concentration of insulin-like growth factor-1 in serum in dairy cows in early lactation and reproductive performance and milk yield. *J. Dairy Sci.* **91**, 3862–3868 [CrossRef Medline](#)
38. Ramer, I., Kanninen, T. T., Sisti, G., Witkin, S. S., and Spandorfer, S. D. (2015) Association of *in vitro* fertilization outcome with circulating insulin-like growth factor components prior to cycle initiation. *Am. J. Obstet. Gynecol.* **213**, 356.e1–6
39. Schmidt, D., Schwalie, P. C., Ross-Innes, C. S., Hurtado, A., Brown, G. D., Carroll, J. S., Flicek, P., and Odom, D. T. (2010) A CTCF-independent role for cohesin in tissue-specific transcription. *Genome Res.* **20**, 578–588 [CrossRef Medline](#)
40. Du, H., and Taylor, H. S. (2015) The role of Hox genes in female reproductive tract development, adult function, and fertility. *Cold Spring Harb. Perspect. Med.* **6**, a023002 [Medline](#)
41. Simmen, R. C., Heard, M. E., Simmen, A. M., Montales, M. T., Marji, M., Scanlon, S., and Pabona, J. M. (2015) The Kruppel-like factors in female reproductive system pathologies. *J. Mol. Endocrinol.* **54**, R89–R101 [CrossRef Medline](#)
42. Kelleher, A. M., Peng, W., Pru, J. K., Pru, C. A., DeMayo, F. J., and Spencer, T. E. (2017) Forkhead box a2 (FOXA2) is essential for uterine function and fertility. *Proc. Natl. Acad. Sci. U.S.A.* **114**, E1018–E1026 [CrossRef Medline](#)
43. Wang, J., Meng, X., Chen, H., Yuan, C., Li, X., Zhou, Y., and Chen, M. (2016) Exploring the mechanisms of genome-wide long-range interactions: interpreting chromosome organization. *Brief. Funct. Genomics* **15**, 385–395 [CrossRef Medline](#)
44. Li, W., Notani, D., and Rosenfeld, M. G. (2016) Enhancers as non-coding RNA transcription units: recent insights and future perspectives. *Nat. Rev. Genet.* **17**, 207–223 [CrossRef Medline](#)
45. Li, W., Notani, D., Ma, Q., Tanasa, B., Nunez, E., Chen, A. Y., Merkurjev, D., Zhang, J., Ohgi, K., Song, X., Oh, S., Kim, H. S., Glass, C. K., and Rosenfeld, M. G. (2013) Functional roles of enhancer RNAs for oestrogen-dependent transcriptional activation. *Nature* **498**, 516–520 [CrossRef Medline](#)
46. Jefferson, W. N., Kinyamu, H. K., Wang, T., Miranda, A. X., Padilla-Banks, E., Suen, A. A., and Williams, C. J. (2018) Widespread enhancer activation via ER α mediates estrogen response in vivo during uterine development. *Nucleic Acids Res.* **46**, 5487–5503 [CrossRef Medline](#)
47. Fujii, W., Kawasaki, K., Sugiura, K., and Naito, K. (2013) Efficient generation of large-scale genome-modified mice using gRNA and CAS9 endonuclease. *Nucleic Acids Res.* **41**, e187 [CrossRef Medline](#)
48. Dobin, A., Davis, C. A., Schlesinger, F., Drenkow, J., Zaleski, C., Jha, S., Batut, P., Chaisson, M., and Gingeras, T. R. (2013) STAR: ultrafast universal RNA-seq aligner. *Bioinformatics* **29**, 15–21 [CrossRef Medline](#)
49. Love, M. I., Huber, W., and Anders, S. (2014) Moderated estimation of fold change and dispersion for RNA-seq data with DESeq2. *Genome Biol.* **15**, 550 [CrossRef Medline](#)
50. Langmead, B., Trapnell, C., Pop, M., and Salzberg, S. L. (2009) Ultrafast and memory-efficient alignment of short DNA sequences to the human genome. *Genome Biol.* **10**, R25 [CrossRef Medline](#)
51. Quinlan, A. R., and Hall, I. M. (2010) BEDTools: a flexible suite of utilities for comparing genomic features. *Bioinformatics* **26**, 841–842 [CrossRef Medline](#)
52. Durand, N. C., Shamim, M. S., Machol, I., Rao, S. S., Huntley, M. H., Lander, E. S., and Aiden, E. L. (2016) Juicer provides a one-click system for analyzing loop-resolution Hi-C experiments. *Cell Systems* **3**, 95–98 [CrossRef Medline](#)
53. Pfaffl, M. W. (2001) A new mathematical model for relative quantification in real-time RT-PCR. *Nucleic Acids Res.* **29**, e45 [CrossRef Medline](#)